https://doi.org/10.36296/1819-8058.2025.4(83).18-33

OPTIMIZED PI CONTROL FOR POWER FLOW AND DC LINK VOLTAGE REGULATION IN A PV-WIND-BATTERY MICROGRID USING GREY WOLF OPTIMIZATION

Received Mar. 21, 2025; accepted Dec. 09, 2025
Available online Dec. 31, 2025

Veera Narasimha Murthy Mogilicharla[1], Gudapati Sambasiva Rao[2]

Author for correspondence: Veera Narasimha Murthy Mogilicharla, e-mail: murthyeps@gmail.com

[1] Research Scholar
https://orcid.org/0009-0003-4371-2104

[2] Professor
https://orcid.org/0000-0001-7410-5911

[1] University College of Engineering and Technology, Acharya Nagarjuna University, Guntur, Andhra Pradesh, India

[2] R.V.R. & J.C. College of Engineering, Chowdavaram, Guntur, Andhra Pradesh, India

Abstract. *Microgrids have become essential in modern power systems, enabling reliable and sustainable energy distribution while operating independently or with the main grid. The growing integration of renewable sources like photovoltaic (PV) and wind energy, along with battery storage, necessitates advanced control strategies for efficient power management and grid stability. This paper presents an optimized power flow control strategy for a PV-Wind-Battery hybrid microgrid using a Voltage Source Converter (VSC) to regulate active and reactive power while maintaining DC link voltage stability. A Proportional-Integral (PI) controller plays a crucial role in ensuring system performance under varying conditions. However, conventional PI tuning is challenging due to the nonlinear nature of renewable energy sources. To overcome this, an optimized tuning approach based on the Grey Wolf Optimization (GWO) algorithm is proposed. Inspired by the social structure and hunting behaviour of grey wolves, GWO efficiently balances exploration and exploitation to determine optimal control gains. The PV system employs Perturb and Observe (P&O) Maximum Power Point Tracking (MPPT), while an adaptive P&O MPPT strategy is used for wind energy to maximize power extraction. The battery storage system dynamically switches between charging and discharging to maintain power balance. The GWO-based PI controller is compared with conventional methods, including Ziegler-Nichols (ZN), Genetic Algorithm (GA), and Particle Swarm Optimization (PSO). Simulation results demonstrate superior transient response, reduced steady-state error, and minimized power fluctuations. Additionally, Total Harmonic Distortion (THD) analysis confirms lower harmonic distortion, enhancing power quality and system reliability, making GWO a promising approach for microgrid optimization.*

Keywords: *Grey Wolf Optimization (GWO), PI Controller Tuning, Power Flow Control, DC Link Voltage Regulation, PV-Wind-Battery Microgrid, Voltage Source Converter (VSC) Control*

ОПТИМІЗОВАНЕ ПРОПОРЦІЙНО-ІНТЕГРАЛЬНЕ КЕРУВАННЯ ДЛЯ РЕГУЛЮВАННЯ ПОТОКУ ПОТУЖНОСТІ ТА НАПРУГИ ПОСТІЙНОГО ЛАНЦЮГА В МІКРОМЕРЕЖІ PV-ВІТРО-АКУМУЛЯТОРНОГО ТИПУ З ВИКОРИСТАННЯМ АЛГОРИТМУ ОПТИМІЗАЦІЇ «СІРИЙ ВОВК»

Отримано 21 бер. 2025 р.; рекомендовано до публікації 09 груд. 2025 р.
Доступно онлайн 31 груд. 2025 р.

Віра Нарасімха Мурті Могиличарла[1], Гудапаті Самбасіва Рао[2]

Автор для кореспонденції: Віра Нарасімха Мурті Могиличарла, e-mail: murthyeps@gmail.com

[1] канд. наук, доцент
https://orcid.org/0009-0003-4371-2104

[2] канд. наук, доцент
https://orcid.org/0000-0001-7410-5911

[1] Університетський коледж інженерії та технологій, Університет Ачар'ї Нагарджуни, Гунтур, Андхра-Прадеш, Индия

[2] Инженерный колледж RVR & JC, Чандрамулипурам, Чоудаварам, Гунтур, Андхра-Прадеш, Индия

Анотація. *Мікромережі стали невід'ємною складовою сучасних енергетичних систем, забезпечуючи надійний і стійкий розподіл електроенергії як у режимі автономної роботи, так і при підключенні до основної мережі. Зростання частки відновлюваних джерел енергії, зокрема фотоелектричних (PV) і вітрових систем, у поєднанні з акумуляторними сховищами потребує вдосконалених стратегій керування для підвищення ефективності енергорозподілу та стабільності мікромережі.*

У цій роботі запропоновано оптимізовану стратегію керування потоком потужності для гібридної мікромережі PV-вітро-акумуляторного типу з використанням перетворювача напруги (VSC), який регулює активну та реактивну потужність, а також стабілізує напругу постійного ланцюга. Ключову роль у забезпеченні стабільної роботи системи відіграє пропорційно-інтегральний (ПІ) регулятор. Проте традиційне налаштування ПІ-регулятора є складним через нелінійність характеристик відновлюваних джерел. Для вирішення цієї проблеми запропоновано використати алгоритм оптимізації «Сірий вовк» (Grey Wolf Optimization, GWO), який ефективно визначає оптимальні коефіцієнти регулятора завдяки поєднанню пошукової та експлуатаційної поведінки.
У PV-системі реалізовано метод відстеження точки максимальної потужності (MPPT) «збурення та спостереження» (Perturb and Observe, P&O), тоді як для вітрової системи застосовано адаптивну стратегію P&O MPPT з метою максимізації виробітку енергії. Акумуляторна система автоматично перемикається між режимами заряджання та розряджання для підтримання енергетичного балансу.
Результати моделювання показали, що ПІ-регулятор, налаштований за допомогою алгоритму GWO, має кращі перехідні характеристики, меншу похибку в сталому режимі та знижені коливання потужності порівняно з традиційними методами налаштування (Ziegler-Nichols, Genetic Algorithm, Particle Swarm Optimization). Аналіз гармонічних спотворень (THD) засвідчив нижчий рівень гармонік, що сприяє підвищенню якості електроенергії та надійності системи.
Таким чином, застосування алгоритму GWO можна вважати перспективним підходом до оптимізації мікромереж у сфері відновлюваної енергетики.

Ключові слова: *алгоритм оптимізації «Сірий вовк» (GWO); ПІ-регулятор; керування потоком потужності; регулювання напруги постійного ланцюга; мікромережа PV-вітро-акумуляторного типу; керування перетворювачем напруги (VSC).*

1. Introduction

The increasing penetration of renewable energy sources (RES), such as photovoltaic (PV) and wind energy, into microgrids has created new challenges in power flow control due to their intermittent and stochastic nature [1]. Effective energy management and control strategies are necessary to ensure the reliability, stability, and efficiency of microgrids integrating PV-wind-battery systems. Traditional proportional-integral (PI) controllers have been widely used in power systems due to their simplicity and ease of implementation [2]. However, selecting optimal PI controller parameters is critical to achieving desired system performance. Conventional tuning methods often fail to provide optimal performance under dynamic conditions, leading to the exploration of optimization techniques for PI tuning [3]. Metaheuristic optimization algorithms have gained significant attention in control system tuning due to their ability to efficiently handle nonlinear, multi-objective, and high-dimensional problems. Grey Wolf Optimization (GWO) is one such nature-inspired optimization algorithm that mimics the hunting behaviour of grey wolves [4]. It has demonstrated superior performance in various engineering applications due to its exploration-exploitation balance and fast convergence properties. A traditional PI controller for power flow control in a hybrid PV-wind-battery microgrid is proposed in [5]. The study demonstrated satisfactory performance under steady-state conditions but showed limitations in handling dynamic load variations and system uncertainties. The lack of optimization techniques in this study resulted in suboptimal controller performance during transient conditions. A PSO-based approach to optimize PI controllers for DC link voltage stabilization was proposed in [6]. While the results showed improved voltage regulation, the study did not consider the impact of communication delays, which are critical in real-world microgrid operations. The use of a Genetic Algorithm (GA) for tuning PI controllers in a PV-wind-battery microgrid was explored in [7]. The GA-optimized controllers exhibited better performance compared to conventional PI controllers, but the computational time required for optimization was significantly high, limiting its practicality for real-time applications. In [8], the authors employed a fuzzy logic-based approach to enhance the performance of PI controllers. The fuzzy-PI controller showed improved adaptability to system uncertainties, but the increased complexity of the design made it less suitable for large-scale microgrid implementations.

In [9], the authors investigated the application of Artificial Bee Colony (ABC) optimization for tuning PI controllers in a microgrid. The study reported improved dynamic response and reduced oscillations in power flow. However, the ABC algorithm's sensitivity to initial parameters and its tendency to converge to local optima were significant drawbacks. In [10], the authors proposed a hybrid optimization technique combining GA and PSO for PI controller tuning. While the hybrid approach showed promising results, the computational complexity and lack of scalability were major limitations. In [11], the authors utilized a Simulated Annealing (SA) algorithm to optimize PI controllers for DC link voltage control. The study demonstrated improved voltage stability but suffered from slow convergence and high computational costs. In [12], the authors focused on the use of Differential Evolution (DE) for PI controller optimization. The DE-based approach showed better performance compared to traditional methods, but its sensitivity to control parameters and difficulty in tuning were notable drawbacks. The application of Ant Colony Optimization (ACO) for tuning PI controllers in a microgrid is investigated in [13]. The ACO-optimized controllers exhibited improved power flow control, but the algorithm's slow convergence and high computational requirements were significant limitations. In [14], proposed a hybrid approach combining fuzzy logic and PSO for PI controller optimization. While the results were promising, the increased complexity and computational overhead made it less practical for real-time applications. In [15], the authors investigated the use of a Teaching-Learning-Based Optimization (TLBO) algorithm for PI controller tuning. The TLBO-based approach showed improved performance in power flow control and DC link voltage regulation, but its lack of robustness under varying operating conditions was a major drawback. In [16], authors proposed a Harmony Search (HS) algorithm for optimizing PI controllers. The study reported improved dynamic response, but the algorithm's sensitivity to parameter settings and slow convergence were significant limitations.

The use of a Cuckoo Search (CS) algorithm for PI controller optimization was explored in [17]. The CS-based approach demonstrated better performance compared to traditional methods, but its high computational cost and difficulty in parameter tuning were notable drawbacks. In [18], a hybrid approach combining GA and fuzzy logic for PI controller tuning was proposed. While the results were promising, the increased complexity and computational requirements made it less suitable for real-time applications. In [19], the use of a Firefly Algorithm (FA) for optimizing PI controllers was investigated. The FA-based approach showed improved performance, but its sensitivity to initial parameters and slow convergence were significant limitations. Despite the contributions of these studies, many of the proposed optimization techniques suffer from drawbacks such as high computational complexity, slow convergence, sensitivity to initial parameters, and lack of robustness under varying operating conditions. In contrast, the Grey Wolf Optimization (GWO) algorithm offers a promising alternative due to its simplicity, fast convergence, and ability to avoid local optima. GWO-based approaches can efficiently optimize PI controllers for power flow control and DC link voltage regulation in microgrids with PV-wind-battery systems. GWO's balance between exploration and exploitation, along with its low computational requirements, makes it a superior choice for real-time applications. By addressing the limitations of existing optimization techniques, GWO can provide a robust and efficient solution for enhancing the performance of PI controllers in microgrids. This paper focuses on the application of GWO for optimizing PI controller parameters to improve power flow control in a microgrid comprising PV, wind, and battery storage. The proposed approach aims to enhance the stability, dynamic response, and power-sharing efficiency of the system under variable generation and load conditions.

2. HYBRID DG SYSTEM (HDGS)

Fig. 1 illustrates the schematic of the hybrid system, which integrates a PV-Wind-Battery configuration.

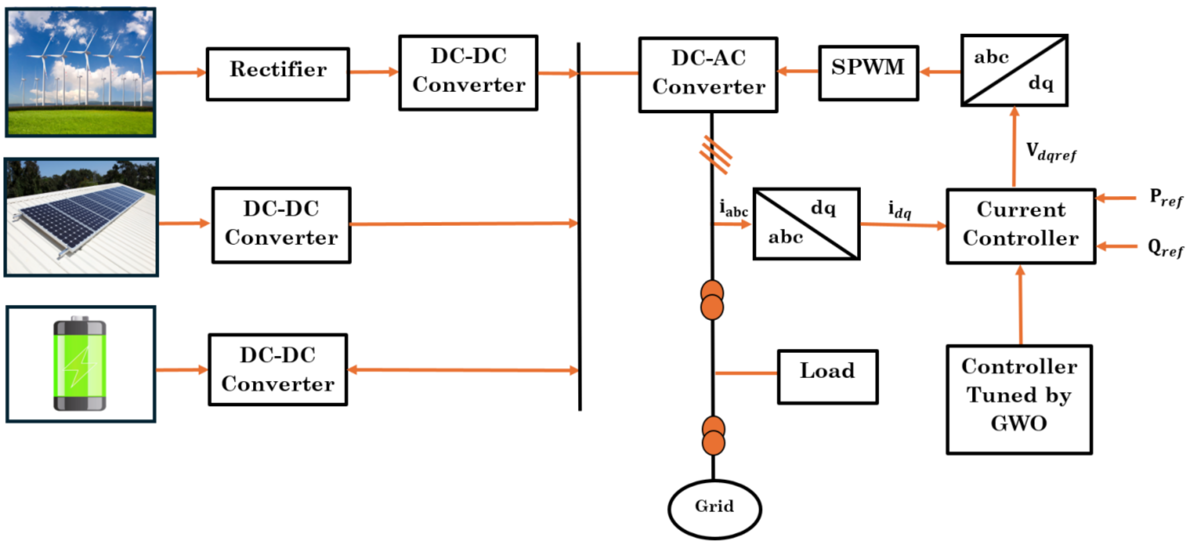

Fig. 1. Management Structure of HDGS with the Proposed Controller

This system comprises a wind turbine, a photovoltaic (PV) system, and a battery, working together to enable efficient energy transfer from the DC bus to the grid. The PV generation system is interfaced with the DC bus via a DC-DC converter operated with Maximum Power Point Tracking (MPPT). Similarly, the wind generation system is connected to the DC bus through a rectifier followed by an MPPT-operated DC-DC converter. The battery storage system is linked to the DC bus through a bidirectional DC-DC converter. The design of the power flow control and management modules for the PV-Wind-Battery system is based on the operational modes of the load and grid. In grid-connected mode, the active and reactive power outputs of the PV-Wind-Battery system are regulated to match their respective reference values. To ensure optimal performance, the voltage source inverter (VSI)-based control system must select an appropriate power control mode. A sinusoidal pulse width modulation (SPWM) technique is employed to regulate the VSI. To meet varying load demands, the power contribution from the main grid and the PV-Wind-Battery system must be dynamically adjusted. Ensuring a consistent supply of active and reactive power requires efficient control of power flow between the PV-Wind-Battery system, the grid, and the load. Furthermore, a reliable integration of power from the main grid and the distributed generation (DG) system is crucial to meeting the load demand [20]. The power balance equation must be satisfied at both the DC-link and the point of common coupling (PCC). The total DC power available at the DC bus from the energy sources in the microgrid is expressed as:

$$P_{dc}(t) = P_{WT}(t) + P_{PV}(t) + P_{Bat}(t) \tag{1}$$

P_{WT}: Power generated by the wind generation system, P_{PV} : Power generated by the solar generation system, P_{bat}: Battery power measured at the output of the respective DC/DC converters, P_{dc}: Total available DC power at the DC bus. The total power generated by renewable sources is determined using Equation (1) and integrated into the overall power flow model. The power balance is calculated by accounting for the outputs of the hybrid energy sources and the load demand at the AC bus.

$$P_g(t) = [P_l(t) - P_{hres}(t)] \tag{2}$$

$$P_l(t) = [P_{hres}(t) + P_g(t)] \tag{3}$$

$$Q_g(t) = [Q_l(t) - Q_{hres}(t)] \tag{4}$$

$$Q_l(t) = [Q_{hres}(t) + Q_g(t)] \tag{5}$$

P_g: Active power supplied by the grid, Q_g: Reactive power supplied by the grid, P_l: Active power consumed by the load, Q_l: Reactive power consumed by the load, P_{hres}: Active power generated by the HDGS, Q_{hres}: Reactive power generated by the HDGS. The battery power of the storage unit is affected by the discharge duration, during which it serves as an energy source, and the charging duration, when it operates as a load. However, maintaining a consistent power balance is challenging due to nonlinear fluctuations on the consumer side and the unpredictable nature of renewable energy sources [21]. To address this challenge, the system unit requires a high-performance operating mode that facilitates efficient power regulation. The active and reactive power, calculated using the direct and quadrature axis voltages and currents, are given by the equations (6) and (7).

$$P_I(t) = \frac{3}{2}\left[v_d * i_d + v_q * i_q\right] \tag{6}$$

$$Q_I(t) = \frac{3}{2}\left[v_q * i_d + v_d * i_q\right] \tag{7}$$

v_d and v_q represent the direct and quadrature axis load voltages, while i_d and i_q denote the direct and quadrature axis load currents.

3. Modelling of sources

3.1. Mathematical formulation of solar PV module

Fig. 2 shows the simplified circuit representation of a solar panel. The PV cell can be modelled as an ideal current source, denoted as $\boldsymbol{I_{ph}}$, with series and parallel resistances, as illustrated in Fig. 2. The output current of an ideal solar cell is expressed in Equation (8).

$$I = I_{ph} - I_d \tag{8}$$

I is PV output current, I_d is diode current, I_{ph} photon current. In semiconductor theory, the fundamental mathematical equation that describes the I-V characteristics of the PV cell is the Shockley diode current equation, as shown in Equation (9).

$$I_d = I_s\left[exp\left(\frac{qV_{oc}}{N_s\,KAT_o}\right) - 1\right] \tag{9}$$

then

$$I_d = I_{ph} - I_s\left[exp\left(\frac{qV_{oc}}{N_s\,KAT_o}\right) - 1\right] \tag{10}$$

I_s is the saturation current, q is the electron charge, $V_{oc}$is the open-circuit voltage, N_s represents the number of series-connected cells per module, K is Boltzmann's constant, and T_o is the nominal cell temperature in Kelvin.

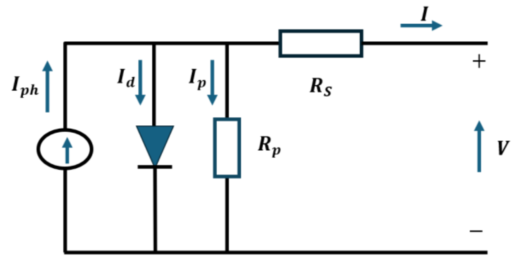

Fig. 2. Equivalent circuit of real model for PV panel

Due to the sensitivity of photovoltaic (PV) generation output to weather conditions such as irradiance and temperature, the use of a DC-DC converter is essential for regulating both the output voltage and power. Fig. 3 highlights the importance of regulating the PV voltage to the maximum power point voltage (V_{mpp}), a crucial factor in maximizing the power output from the PV arrays using a DC-DC converter. As shown in Fig. 3, controlling the PV voltage to reach V_{mpp} is crucial for optimizing power extraction from the PV arrays through the DC-DC converter. The P&O MPPT (Perturb and Observe Maximum Power Point Tracking) algorithm is used to generate the duty cycle required for the DC-DC converter to maximize power extraction. Fig. 4 shows the DC-DC converter employed for the PV array.

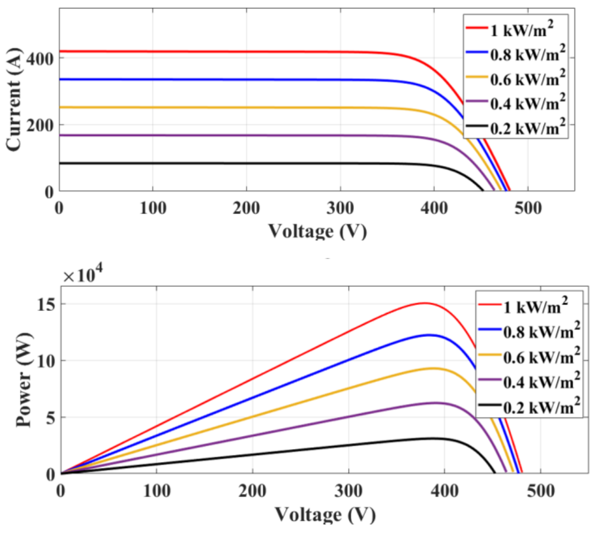

Fig. 3. I-V and P-V characteristics of PV Array

The Perturb and Observe (P&O) algorithm is a commonly used MPPT technique in PV systems. It is a straightforward and effective method for continuously adjusting the operating point of a PV system to ensure it operates at its maximum power point (MPP), where the power output is optimized.

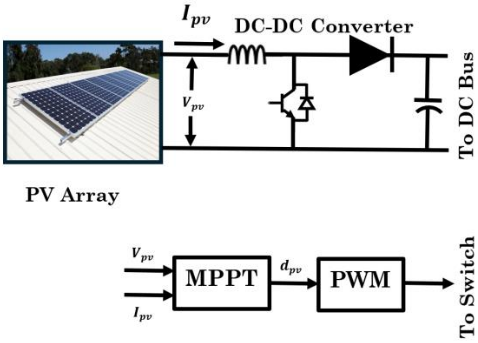

Fig. 4. PV system with boost converter

3.2. PMSG and Wind Turbine

Output power from wind turbine (P_{ω}) is given as in Equation (11)

$$P_{\omega} = \frac{1}{2}\rho A C_p(\lambda, \beta) V_{\omega}^3 \quad (11)$$

ρ is the air density, A is the wind turbine swept area in m^2, λ is the tip speed ratio, and β is the pitch angle. The tip speed ratio λ is defined as the ratio of the blade tip speed ω, the wind turbine blade radius r, and the wind speed V, and it can be expressed by Equation (12).

$$\lambda = \frac{r_{\omega}}{V_{\omega}} \quad (12)$$

Therefore, the mechanical energy generated by wind turbines can be controlled by adjusting both λ and β. For a given β, there is a corresponding power coefficient (C_p) vs. tip speed ratio (λ) curve, where each curve has an optimal C_p value, denoted as $C_{p\,opt}$, which corresponds to the optimal tip speed ratio, λ_{opt}. By controlling these parameters, the mechanical energy of the turbine can be adjusted to align with the available wind speed, with the maximum $C_p$achieved at the optimized rotational speed when βequals zero.

The power generated by the PMSG can be regulated using a DC-DC converter, which is controlled by an MPPT algorithm. Before the DC-DC boost converter takes over the regulation, the PMSG's output is first connected to a diode bridge rectifier. To enhance the dynamic performance of the wind generation system, an adjustable step size ($P\&O$) algorithm is employed to control and manage the DC-DC converter. This approach ensures that the system achieves its peak power output. Unlike traditional P&O algorithms, this adaptive method addresses several limitations that can negatively impact the performance of the wind generation system, particularly in systems with inertia. Traditional P&O algorithms face significant challenges in selecting the optimal step size for rotor speed adjustments.

The optimal rotor speed can be calculated using Equation (13), as shown below:

$$\omega_{opt\_m} = \frac{\lambda_{opt} V_w}{R} \quad (13)$$

λ_{opt} optimal tip speed ratio, ω_{opt_m} is directly related to wind speed expressed in Equation (14)

$$\omega_{opt\_m_p} = \omega_{base\_m} \frac{\upsilon_w}{\upsilon_{base}} \quad (14)$$

υ_{base} refers to the reference wind speed, ω_{base_m}represents the rotor speed at the reference wind speed, $\omega_{opt_m_p}$indicates the current optimal generator speed, and υ_w represents the current wind speed. The control system will make substantial corrections to the rotor speed when it deviates from the required optimal speed. As the rotor speed approaches the desired level, the adaptive ratio R_{adp} will decrease until the optimal speed is reached and maintained, as shown in Equation (15).

$$R_{adp} = K_{per}\left(\frac{\omega_{opt\_m_p} - \omega_m}{\omega_{opt\_m_p}}\right) \quad (15)$$

The perturbation constant K_{per}determines the accuracy in achieving the maximum power output. Once the algorithm determines the ideal rotor speed, a PI controller is used to generate a reference torque to maintain the PMSG rotor at its optimal speed τ_{opt_m}. After that, the input current

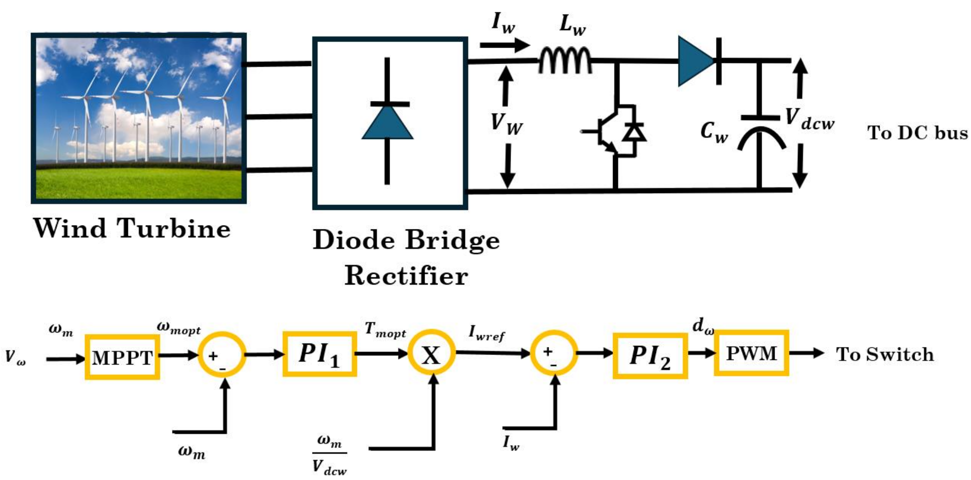

Fig. 5. Wind generation system with boost converter

reference (I_{wref}) for the DC-DC converter is calculated from the torque reference, as shown in Equation (16).

$$I_{wref} = \tau_{opt\_m} \frac{\omega_m}{V_{dcw}} \quad (16)$$

A DC current regulator with PI control is used to maintain the output voltage of the DC-DC converter. This regulator generates the required duty cycle to control the IGBT switch. Fig. 5 illustrates the wind system with the DC-DC converter. The output of the PI_1controller is the reference torque τ_{opt_m}, which is given in Equation (17).

$$\tau_{opt_m} = K_{p1}\left(\omega_{opt_m}(t) - \omega_m(t)\right) + K_{i1}\int\left(\omega_{opt_m}(t) - \omega_m(t)\right)dt \quad (17)$$

K_{p1} and K_{i1} are PI controller gains

Output of the PI_2 controller is duty cycle (d_w) required by the converter which is given as

$$d_w = K_{p2}\left(I_{Wref}(t) - I_W(t)\right) + K_{i2}\int\left(I_{Wref}(t) - I_W(t)\right)dt \quad (18)$$

K_{p2} and K_{i2} are PI controller gains

3.3. Battery energy storage system (BESS*)*

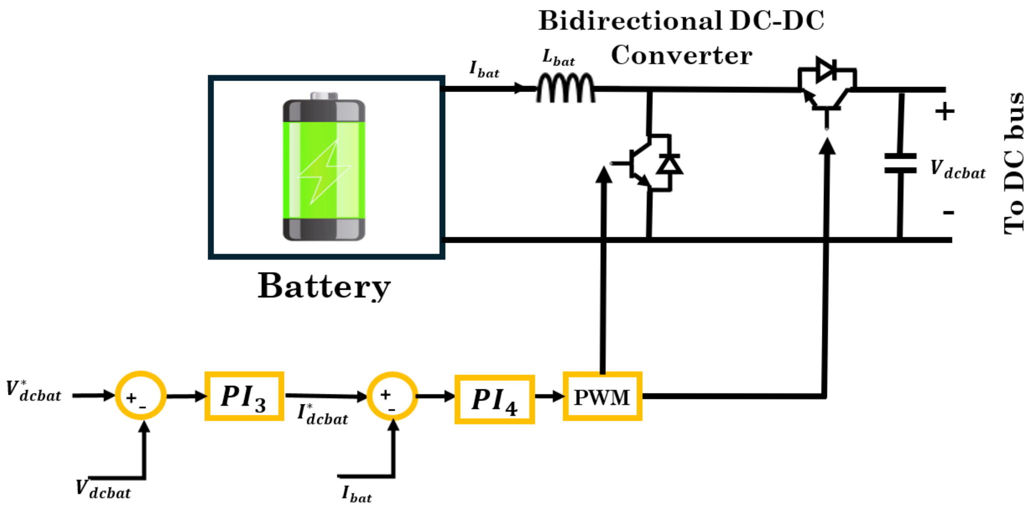

Fig. 6. Battery storage system with DC-DC converter

Bidirectional DC DC converter of battery storage system regulate the DC voltage across DC bus. DC bus voltage can be taken as feedback and compared with reference DC voltage to generate reference DC current. As shown in Fig. 6, the output of the PI_3 controller is the reference battery current I_{batref}, which is given in Equation (19).

$$I_{batref} = K_{p3}\left(V_{batref}(t) - V_{dcbat}(t)\right) + K_{i3}\int\left(V_{batref}(t) - V_{dcbat}(t)\right)dt \quad (19)$$

K_{p3} and K_{i3} are PI controller gains, V_{batref} battery reference voltage, V_{dcbat} actual battery voltage, Output of the PI_4 controller is duty cycle of the switches in bidirectional converter which is given as in Equation (20)

$$d_{bat} = K_{p4}\left(I_{batref}(t) - I_{bat}(t)\right) + K_{i4}\int\left(I_{batref}(t) - I_{bat}(t)\right)dt \quad (20)$$

K_{p4} and K_{i4} are PI controller gains, I_{batref} battery reference current, I_{bat} actual battery current,

3.4. Current Control Strategy of DC-AC converter

Fig. 7 presents the control strategy of the DC-AC converter.

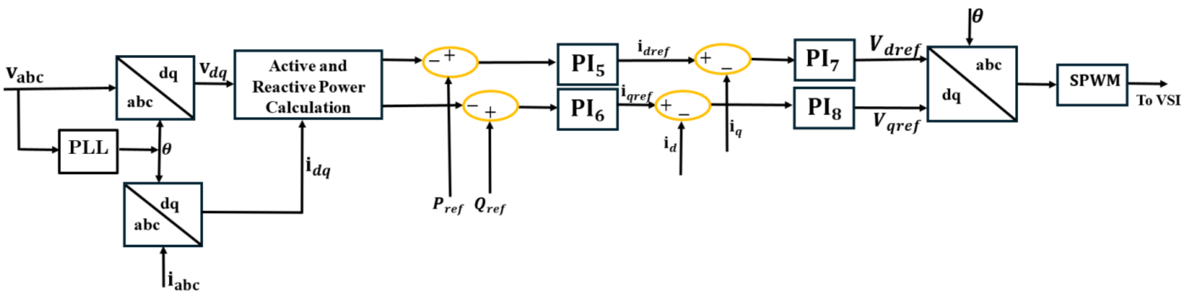

Fig. 7. Control Strategy of the DC-AC converter

Equations (21) and (22) show the reference current used to achieve the control goal. The two PI controllers in the power controller work with the external control loop to generate the reference current vectors i_{dref} and i_{qref}.

$$i_{dref} = K_{p5}\left(P_{ref}(t) - P(t)\right) + K_{i5}\int\left(P_{ref}(t) - P(t)\right)dt \quad (21)$$

$$i_{qref} = K_{p6}\left(Q_{ref}(t) - Q(t)\right) + K_{i6}\int\left(Q_{ref}(t) - Q(t)\right)dt \quad (22)$$

K_{p5} and K_{i5} are PI controller gains, P_{ref} reference active power, Q_{ref} reference reactive power, P actual active power and Q actual reactive power.

The controller's output is important for accurate tracking and reducing inverter ripple. This is achieved by using two PI controllers to correct current errors, along with feedback from the inverter current and feedforward from the grid voltage, improving both steady-state and dynamic performance. The controller uses a PWM system to generate voltage vectors with reduced harmonic distortion. In addition to the PWM system, it includes a current feedback loop and a grid voltage feedforward loop to enhance both steady-state and dynamic performance. These loops help eliminate current errors, ensure precise tracking, and reduce inverter drift, as shown in Equations (23) and (24).

$$v_{dref} = K_{p7}\left(i_{dref}(t) - i_d(t)\right) + K_{i7}\int\left(i_{dref}(t) - i_d(t)\right)dt \quad (23)$$

$$v_{qref} = K_{p8}\left(i_{qref}(t) - i_q(t)\right) + K_{i8}\int\left(i_{qref}(t) - i_q(t)\right)dt \quad (24)$$

K_{p7} and K_{i7} are PI controller gains, i_{dref} reference direct axis current, i_{qref} reference quadrature axis current, i_d actual direct axis current and i_q actual quadrature axis current.

In grid-connected mode, the HDGS unit controls both the size and phase of the inverter current to supply the required active and reactive power to the grid. The control strategy for active and reactive power in the HDGS unit is based on frequency and voltage regulation. To assess the performance of the HDGS unit, the outputs from the PV irradiance, wind turbine, and battery are considered. Tuning the PI controller gains is important for ensuring effective and stable control of a system. PI controllers are often used to regulate a process variable. Heuristic optimization algorithms can be used to automate the process of tuning a PI controller. These algorithms search through the parameter space to find the best controller settings that minimize performance issues like integral of time-weighted absolute error (ITAE), overshoot, or settling time. These algorithms search for the best controller settings to reduce performance issues like ITAE, overshoot, or settling time. When using heuristic optimization algorithms for tuning a PI controller, it's important to set the objective function based on the specific performance goals of the control system. Also, the algorithm parameters (like population size and mutation rate) need to be carefully chosen and adjusted for the application. Running multiple optimization trials and analyzing the results can help ensure that the controller settings are both robust and reliable.

The goal of design optimization is to find the best design by minimizing an objective function, adjusting design variables, and following given constraints. Sometimes, there are multiple design criteria or objectives to consider at once. In these cases, the design problem becomes a multi-objective optimization challenge. Unlike traditional optimization methods that focus on one objective, multi-objective optimization is different. Traditional methods can't handle the complexity of optimizing multiple conflicting objectives at the same time. That's why specialized techniques for multi-objective optimization are needed to deal with these complex design problems.

Multi Objective optimization can be defined as shown in Equations (25) to (28)

$$\min F(x,k) = [F_1 F_2 \dots F_n]^T \quad (25)$$

$$u(x,k) \le 0 \quad (26)$$

$$v(x,k) = 0 \quad (27)$$

$$x_{i,lb} \le x_i \le x_{i,ub}(i = 1,2 \dots d) \quad (28)$$

Consider the objective function vector F, which depends on the design vector x and a constant parameter vector p. The inequality and equality constraints are represented by u and v. Also, $x_{i,lb}$ and $x_{i,ub}$ show the lower and upper limits for the ith design variable. The most common method for multi-objective optimization is the weighted sum method. The most common method for multi-objective optimization is the weighted sum method. In this approach, multiple objectives are combined into one single objective by assigning a weight to each objective and then adding them together. In short, the combined objective function is a weighted sum of the individual objectives, creating a unified optimization criterion represented as $F_{objective}$in Equation (29).

$$F_{objective} = a_1F_1 + a_2F_2 + \dots + a_nF_n \quad (29)$$

Where $a_1, a_2 \dots, a_n$ are the weights for each objective function. If the sum of the weights equals 1 $\sum_{i=1}^{n} a_i = 1$ and $0 \le a_i \le 1$, the weighted sum is a convex combination of the objectives. In this case, each optimization of a single objective finds a specific optimal solution along the Pareto front. The weighted sum method then adjusts the weights to explore different solutions, producing various optimal points. In this study, the optimization of PI controller gains is performed by using the Integral of Time-weighted Absolute Error (ITAE) as the sole objective function. The objective function to be minimized is defined as the sum of the integral of the absolute error multiplied by time for each individual PI controller. The optimization aim is to minimize the total ITAE, improving the dynamic response and overall performance of the control system. The final objective function to be minimized is expressed in Equation (30).

$$F_{objective} = a_1 ITAE_1 + a_2 ITAE_2 + \dots + a_n ITAE_n \quad (30)$$

The Grey Wolf Optimization is used to optimize the Proportional-Integral (PI) controller gains (proportional gain and integral time constant). The goal of this optimization is to improve the dynamic response of the system. The goal is to optimize all eight PI controller gains: two PI controllers regulate the boost converter in the wind generation system, another two control the bidirectional converter in the battery storage system, and the remaining four manage the DC-AC converter. This optimization aims to improve control overactive and reactive power, as well as enhance the regulation of DC and AC side voltages. The PI controller gains to be optimized include $K_{p1}, K_{p2}, \dots K_{p8}$representing the eight proportional gains, and $K_{i1}, K_{i2}, \dots K_{i8}$which represent the integral time constants.

4. Grey Wolf Optimizer

The Grey Wolf Optimizer (GWO) is a population-based metaheuristic algorithm inspired by the social behaviour of grey wolves, first introduced by Mirjalili et al. in 2014 [22]. This algorithm simulates both the leadership structure and the cooperative hunting strategies of grey wolves in their natural habitat. Grey wolves typically live in packs with a distinct hierarchy, as depicted in Fig. 8.

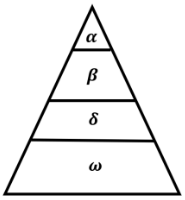

Fig. 8. Hierarchy of a grey wolf pack (Mirjalili et al., 2014) [22]

4.1. Mathematical model

Let M represent the number of wolves in the pack and let $X_i = [X_1, X_2, \dots, X_k]$ denote the position vector of the i-th wolf, where K is the dimensionality of the problem being addressed. The model used to update each wolf's position based on the encircling behaviour is given by Equations (31) and (32).

$$D = |C.X_P(t) - x(t)| \tag{31}$$

$$x(t+1) = X_P(t) - A.D \tag{32}$$

Here, t represents the current iteration, $x(t)$ denotes the wolf's current position, and $X_P(t)$ is the prey's position. The vectors A and C are calculated using Equations (33) and (34), respectively.

$$A = 2.ar_1 - a \tag{33}$$

$$C = 2.r_2 \tag{34}$$

$$a = 2 - \left(iter \times \left(\frac{2}{Max_{iter}}\right)\right) \tag{35}$$

Here, r_1 and r_2 are random vectors with values in the range [0,1], and a is a vector whose components decrease linearly from 2 to 0 throughout the algorithm's execution. Fig. 9(a) shows the encircling behaviour of wolves during a hunt in a 2D scenario. Each wolf updates its position based on the estimated location of the prey and can move to various new positions depending on the vectors A and C. However, the precise location of the prey (i.e., the optimal solution to the problem at hand) remains unknown. As previously noted, the hunting process is directed by the α, β, and δ wolves. To model this characteristic, the GWO algorithm assumes that the α, β, and δ wolves—representing the candidate solutions with the best fitness values—have a more precise understanding of the prey's location. Consequently, the position of each wolf is updated based on the positions of the α, β, and δ wolves, as illustrated in Equations (36–42).

$$D_\alpha = |C_1.X_\alpha - X| \tag{36}$$

$$D_\beta = |C_1.X_\beta - X| \tag{37}$$

$$D_\delta = |C_1.X_\delta - X| \tag{38}$$

$$X_1 = X_\alpha - A_1 D_\alpha \tag{39}$$

$$X_2 = X_\beta - A_2 D_\beta \tag{40}$$

$$X_3 = X_\delta - A_3 D_\delta \tag{41}$$

$$X(t+1) = X_1 + X_2 + X_3 \tag{42}$$

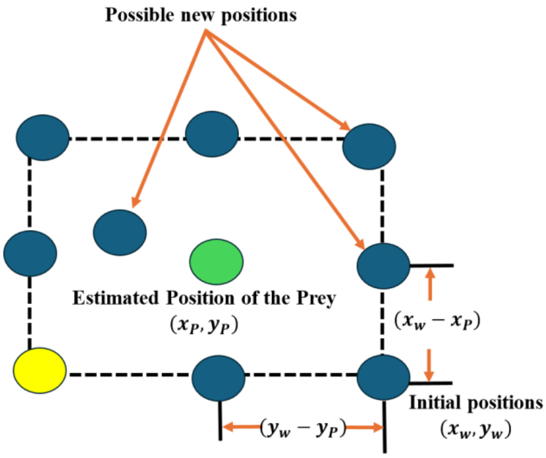

(a)

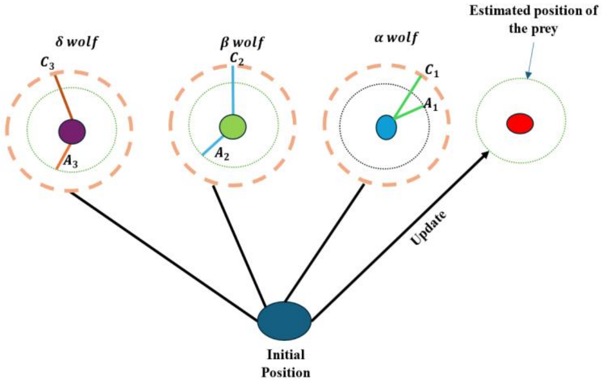

(b)

Fig. 9. (a) Encircling behaviour of a pack (b) Position update in the grey wolf optimizer algorithm (adapted from Mirjalili et al., 2014)

Fig. 9 (b) depicts the process of updating the positions of the wolves. Algorithm 1 provides the pseudocode for implementing the GWO algorithm.

Grey Wolf Optimization (GWO) Algorithm

Initialize population (X) of grey wolves randomly in search space
Define maximum number of iterations (Max_iter), the number of wolves (n) and problem dimension (d)
Calculate fitness of each wolf in the population
Identify X_α (best), X_β(second best), and X_δ (third best) wolves
Start main optimization loop
for $iter\ =\ 1\ to\ Max\_iter$
    Update the positions of the remaining wolves for each wolf i in the population for each dimension j
        for each wolf i in the population
            for each dimension j
                Compute coefficients $a, A\ and\ C$
                Compute distances to $\alpha, \beta\ and\ \delta\ (D_\alpha, D_\beta\ and\ D_\delta)$
                Compute new position X_{new} using $X_1, X_2\ and\ X_3$
            end
        end
    Apply boundary constraints
    Evaluate new fitness values
    Update X_α (best), X_β(second best), and X_δ (third best) based on new fitness values
    Replace old population with new positions
    Store the best solution found so far
    Best Solution = Alpha
end
Output the best solution
Return Best Solution

5. Simulation Results

This section presents simulation results validating the effectiveness of the proposed GWO-based control method. A key performance metric is maintaining DC bus voltage and active/reactive power within specified ranges under different Microgrid (MG) operating modes. Simulations are conducted in MATLAB/SIMULINK, with system specifications shown in Table 1. To demonstrate superiority, GWO is compared with Genetic Algorithm [23], PSO [24], and Ziegler-Nichols (ZN) [25]. The control strategy from Section 3 is applied to the system in Fig. 1, using optimized PI gains. Table 2 presents these gains for different algorithms. Three test cases evaluate the proposed method: (1) Irradiance, temperature and wind speed changes, (2) reference active and reactive power changes, and (3) Load changes. Fig. 10 (a) presents the comparison of active and reactive power tracking performance with proposed GWO and conventional ZN, GA and PSO algorithms. Fig. 10 (b) presents the comparison of DC link voltage tracking performance with proposed GWO and conventional ZN, GA and PSO algorithms. Tuned PI controller gains are presented in Table 2. Comparison of performance indices between proposed algorithm and conventional algorithms from literature is presented in Table 3.

Table 1. Parameters of the Hybrid DG system

Parameter	**Value**
PV Array	
Manufacturer and Model	LG, LG350N2W-B3
Open Circuit Voltage (V_{oc})	48,1 V
Short Circuit Current (I_{sc})	9,74 A
Maximum power point voltage (V_{mpp})	37,9 V
Maximum power point current (I_{mpp})	9,24 A
Series-connected modules per string	43
Parallel strings	10
PMSG	
Stator Resistance	0,8634
Stator Inductance	0,8121 μH
Torque Constant	4,82
Inertia	0,0027
Wind Turbine	
Mechanical output power	150 kW
Base wind speed	11 m/s
Rotor diameter	24,5 m
Swept rotor area	480 m^2
Battery	
Nominal voltage	600
Rated capacity	800
Grid	**11 kV, 50 Hz**

6.1. Case 1: Analysis of Irradiance, Temperature, and Wind Speed Variations

In this case, variations in irradiance, temperature, and wind speed are analysed to assess their impact on the generated power from the photovoltaic (PV) and wind energy systems. The power output from the PV system is directly influenced by the irradiance and temperature levels, while the power generated by the wind system depends on the variations in wind speed. The irradiance and temperature start at 200 W/m² and 30°C, respectively, from 0 to 4 seconds. These values then increase to 400 W/m² and 32°C, followed by further increments to 600 W/m² and 34°C between 4 to 8 seconds. The irradiance continues to rise to 800 W/m² and 36°C between 8 to 12 seconds and finally reaches 1000 W/m² and 38°C at 12 to 20 seconds.

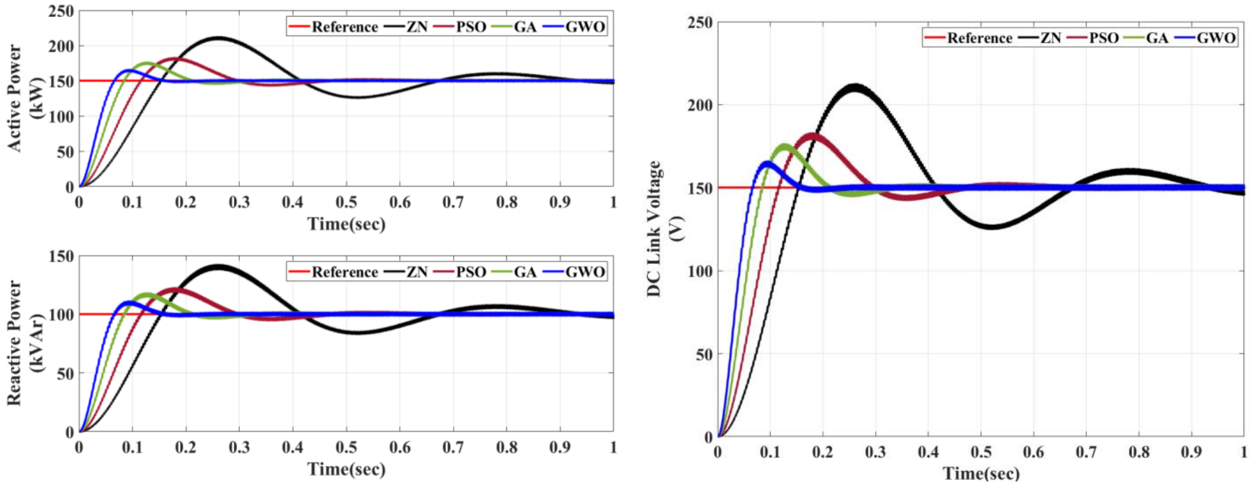

(a) *(b)*

Fig. 10. (a) active and reactive power comparison (b) DC link voltage comparison

Table 2. Optimized gains of PI controllers using proposed and various algorithms

Algorithm	K_{p1}, K_{i1}	K_{p2}, K_{i2}	K_{p3}, K_{i3}	K_{p4}, K_{i4}	K_{p5}, K_{i5}	K_{p6}, K_{i6}	K_{p7}, K_{i7}	K_{p8}, K_{i8}
Proposed GWO	0,8221 5,9568	1,8265 4,4410	0,9588 1,0731	1,7920 2,2863	0,2962 1,4625	1,0033 1,4135	0,9098 2,5126	0,5197 2,2459
PSO	0,4517 7,9595	2,1464 5,1731	0,7417 1,0570	1,6142 2,.6405	0,1328 1,5571	0,7457 2,4346	1,5295 1,9126	1,1673 1,9816
GA	0,6283 7,3236	2,0684 5.0611	0,7837 1,6274	1,0361 2,5383	0,3039 1.8097	0,49590 2.09410	1,6852 2.9816	1,3414 2.7502
Ziegler Nicholas	0,6695 7,7959	1,63765 4,4723	0,7403 1,1844	0,6690 2,9526	0,33917 2,2928	0,5989 2,0129	1,4019 3,2008	1,6861 2,7817

Table 3. Comparison of performance indices between proposed algorithm and previous algorithms from literature

Algorithm	DC Bus Voltage				Active Power				Reactive Power			
	IAE	ISE	ITAE	ITSE	IAE	ISE	ITAE	ITSE	IAE	ISE	ITAE	ITSE
Proposed GWO	0,0514	0,0279	0,0167	0,01264	0,0598	0,0477	0,0149	0,0037	0,0451	0,0342	0,0135	0,0146
PSO	0,0456	0,0212	0,0213	0,0056	0,0353	0,0354	0,0028	0,0037	0,0381	0,01827	0,01588	0,01957
GA	0,04881	0,03369	0,01573	0,01690	0,04378	0,03715	0,01100	0,00872	0,04631	0,02157	0,01105	0,01088
Ziegler Nicholas	0,12596	0,05242	0,03170	0,02325	0,17925	0,09551	0,04475	0,00988	0,19109	0,096691	0,054999	0,01500

Similarly, the wind speed varies dynamically over time, beginning at 8 m/s from 0 to 3 seconds, increasing to 9 m/s between 3 to 6 seconds, and further rising to 10 m/s from 6 to 8 seconds. It continues increasing to 11 m/s between 8 to 12 seconds and peaks at 12 m/s from 12 to 15 seconds. After this peak, the wind speed starts decreasing, first dropping to 10 m/s between 15 to 18 seconds, and finally reducing back to 8 m/s from 18 to 20 seconds. These variations in irradiance, temperature, and wind speed are illustrated in Fig. 11 (a). The impact of these variations on the power generated by the PV and wind systems is shown in Fig. 11 (b). The power output from the PV system is directly proportional to irradiance and temperature, while the wind power is proportional to wind speed. As the irradiance and temperature increase, the PV system generates more power, and similarly, the wind system produces higher power as wind speed increases. However, the battery power output is governed by the reference active and reactive power settings provided to the voltage source converter (VSC). In the initial phase, when the total power generated by PV and wind systems is insufficient to meet the reference power demand of the VSC, the battery discharges to supply the shortfall. This is indicated by the positive battery terminal power before 8 seconds, which implies that the battery is in a discharging state. As the irradiance and wind speed continue to increase, leading to higher power generation from PV and wind sources, the total generated power exceeds the reference value after 8 seconds. At this point, the battery enters a charging state, and its terminal power turns negative. The battery's state of charge (SOC) increases during this phase, as shown in Fig. 14, whereas during the discharging phase, the SOC decreases.

The reference active and reactive power values provided to the VSC control strategy are set at 150 kW and 100 kVAr, respectively, as depicted in Fig. 12 (a). To maintain these power levels at the VSC AC terminals, the sum of power from PV, wind, and battery must match these reference values. Up to 8 seconds, when PV and wind generation are lower than the reference demand, the battery compensates by discharging. After 8 seconds, as PV and wind generation exceed the reference requirement, the battery starts charging. The effectiveness of the VSC in maintaining the reference power levels is further validated through Fig. 12 (b), which illustrates the active and reactive power consumed by the connected load. The load power requirements are 250 kW of active power and 120 kVAR of reactive power. However, the VSC provides only 150 kW and 100 kVAR, as dictated by the reference inputs. The remaining power required by the load is sourced from the grid, as demonstrated in Fig. 13 (a).

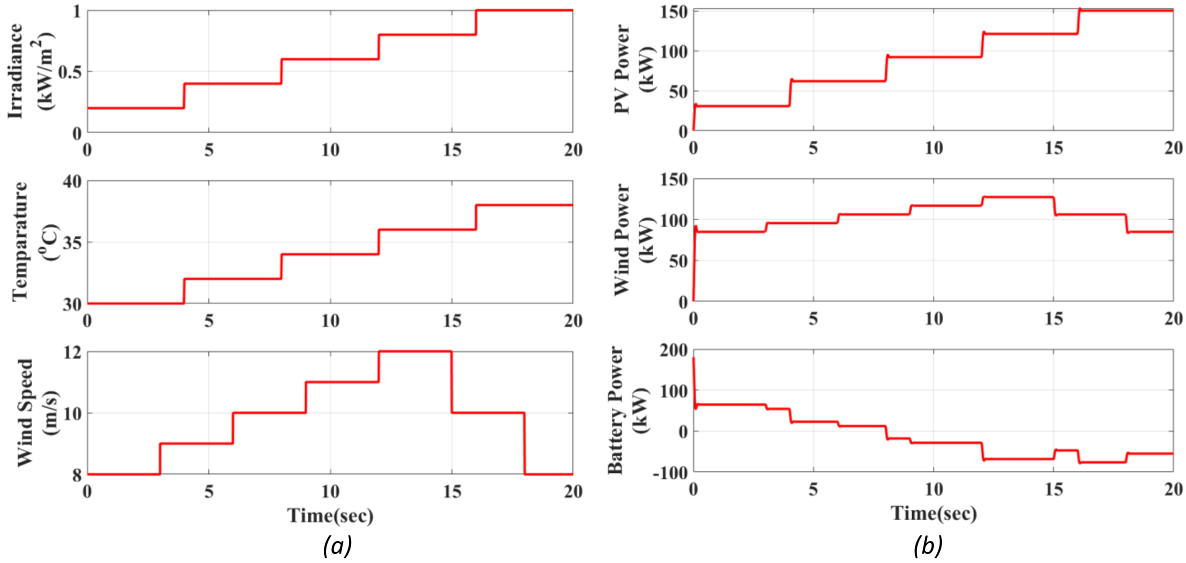

Fig. 11. (a) Irradiance, temperature input to the PV system and wind speed input to the wind generation system (b) generated power from PV, wind and terminal power of the battery

Maintaining a stable DC link voltage is crucial for the proper operation of the VSC and the overall system. Fig. 13 (b) shows the DC link voltage and its reference value. The VSC control strategy effectively regulates the DC voltage, ensuring that it remains within acceptable limits despite fluctuations in power generation and demand. Additionally, power quality is an essential aspect of system performance. The total harmonic distortion (THD) levels of different components in the system are presented in Fig. 15 (a–c).

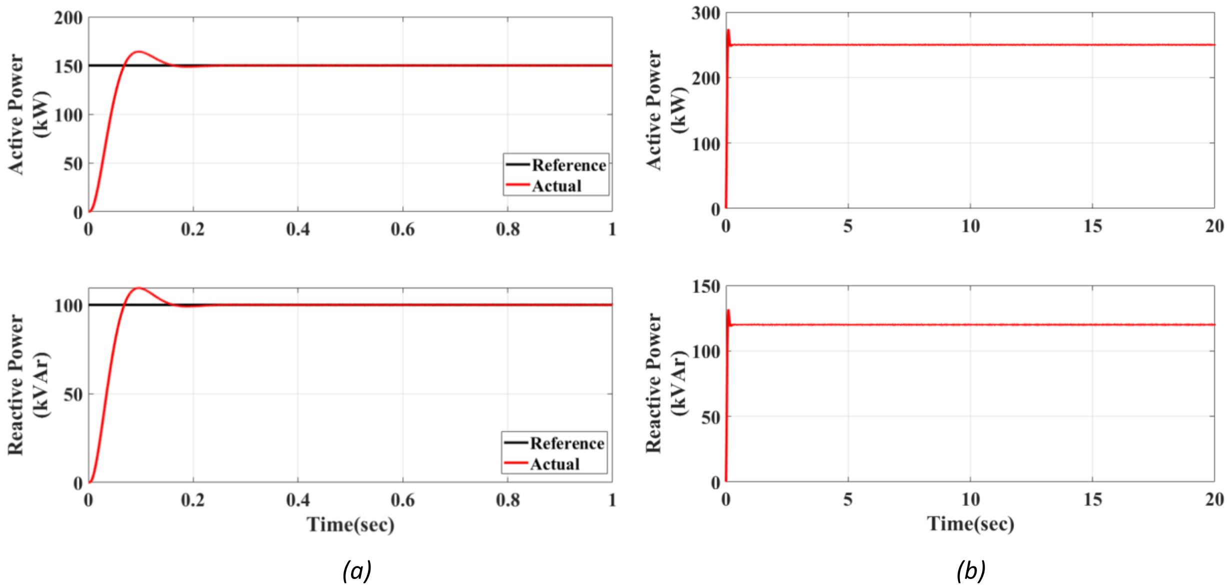

Fig. 12. (a) Reference and actual active and reactive power converted by the VSC (b) Load active and reactive powers

The THD of the load current is 1.99%, the THD of the VSC current is 1.94%, and the THD of the grid current is 1.28%. These values indicate that the proposed control strategy ensures minimal distortion, thereby improving the overall power quality of the system. The analysis of Case 1 demonstrates the impact of irradiance, temperature, and wind speed variations on a hybrid energy system comprising PV, wind, and battery storage. The system effectively balances power generation and demand by utilizing battery storage to compensate for generation shortfalls and surplus energy. The VSC maintains reference active and reactive power levels while ensuring stable DC link voltage. Moreover, the THD values confirm the effectiveness of the control strategy in maintaining power quality within permissible limits.

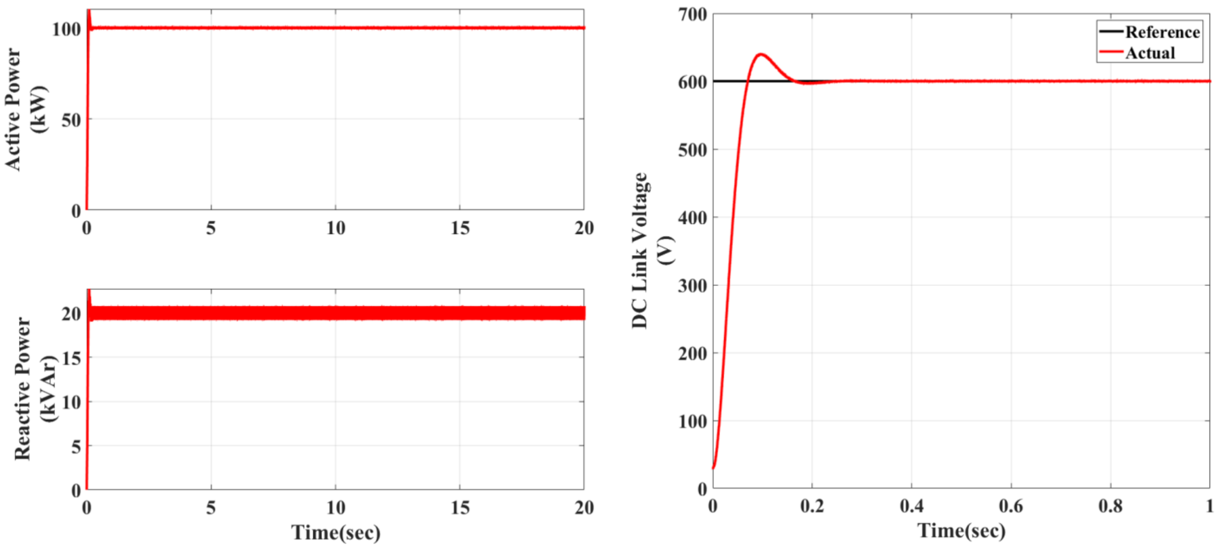

(a) *(b)*

Fig. 13. (a) Active and reactive powers provided by the grid (b) DC Link Voltage

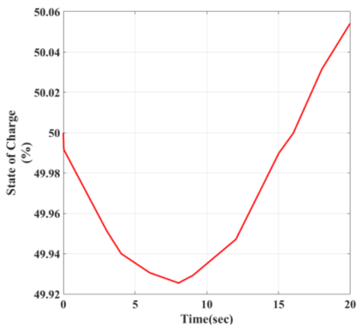

Fig. 14. State of charge of the battery in %

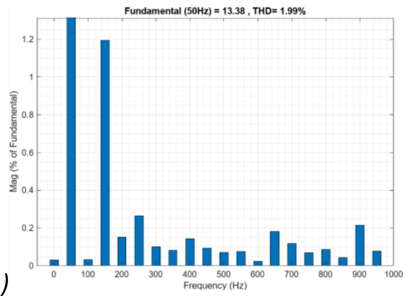

(a)

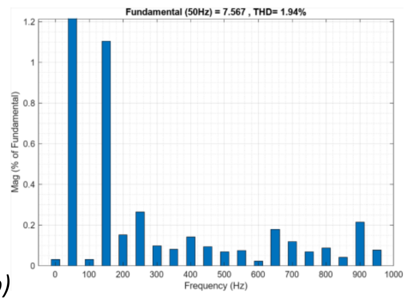

(b)

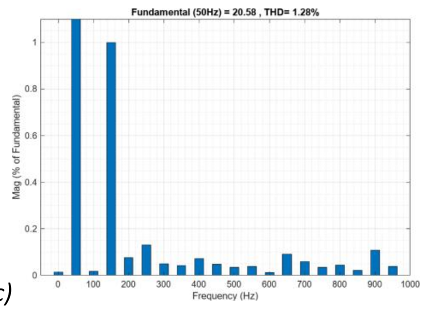

(c)

Fig. 15. (a) load current (b) VSC current and (c) grid current THDs

6.2. Case 2: Analysis of reference active and reactive power variations

In this case, the irradiance, temperature, and wind speed are considered constant throughout the simulation. As a result, the power generated from both the photovoltaic (PV) and wind energy systems remains unchanged. The primary objective of this case is to evaluate the efficacy of the tuned PI controller gains optimized using the GWO algorithm by varying the reference active and reactive power inputs to the control strategy of the VSC.As shown in Fig. 16 (a), the system operates under a constant irradiance of 1000 W/m², a temperature of 34°C, and a wind speed of 12 m/s. These constant environmental conditions ensure that the power outputs from the PV and wind generation systems remain stable, eliminating any fluctuations caused by external weather changes. This allows for a focused assessment of the PI controller's performance under dynamically changing power reference conditions.

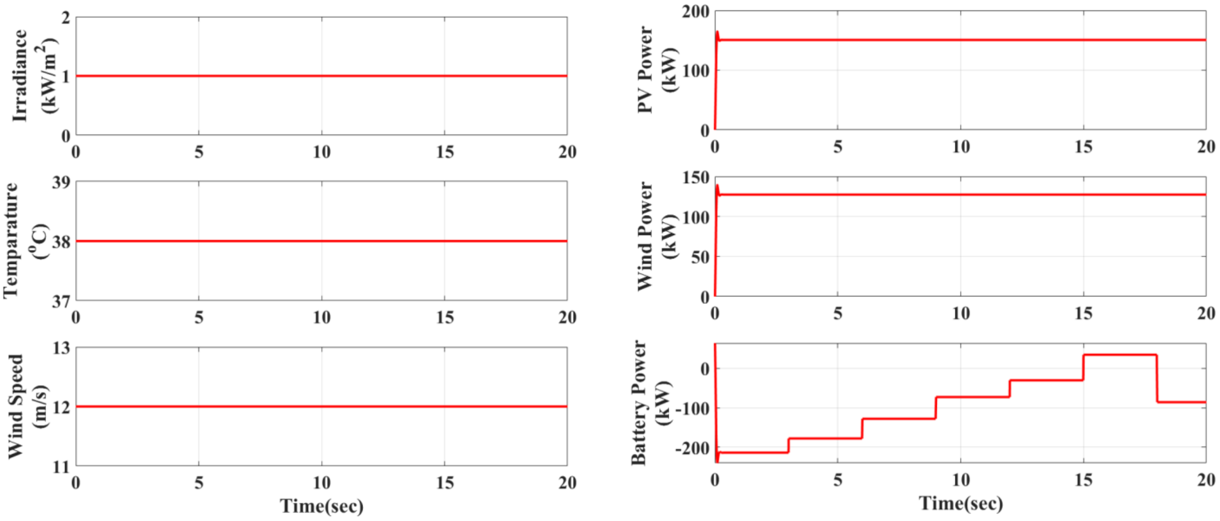

(a) *(b)*

Fig. 16. (a) Irradiance, temperature input to the PV system and wind speed input to the wind generation system (b) generated power from PV, wind and terminal power of the battery

The power outputs from the PV and wind systems, along with the battery terminal power, are illustrated in Fig 16 (b). Since the power generated from PV and wind remains constant, the battery terminal power is adjusted dynamically based on the reference power inputs to the VSC control strategy. The reference active and reactive power values are varied as follows: 0 to 3 seconds: 50 kW and 40 kVAr, 3 to 6 seconds: 80 kW and 60 kVAr, 6 to 9 seconds: 120 kW and 90 kVAr, 9 to 12 seconds: 150 kW and 140 kVAr, 12 to 15 seconds: 180 kW and 140 kVAr, 15 to 18 seconds: 240 kW and 200 kVAr, After 18 seconds: 150 kW and 120 kVAr. To achieve these reference power levels at the AC terminals of the VSC, the battery's terminal power must be adjusted accordingly, as depicted in Fig. 16(b). The battery's operation depends on the relationship between the total power generated from PV and wind and the reference power demand. Before 15 seconds and after 18 seconds, the total power generated by PV and wind exceeds the reference power demand. As a result, the excess power is stored in the battery, putting it in a charging mode. However, between 15 to 18 seconds, the reference power demand surpasses the power generated by PV and wind. In this scenario, the battery enters a discharging mode, supplying the additional required power. This dynamic adjustment ensures that the system maintains a balance between power generation and consumption. The reference and actual powers converted by the VSC are presented in Fig. 17 (a).

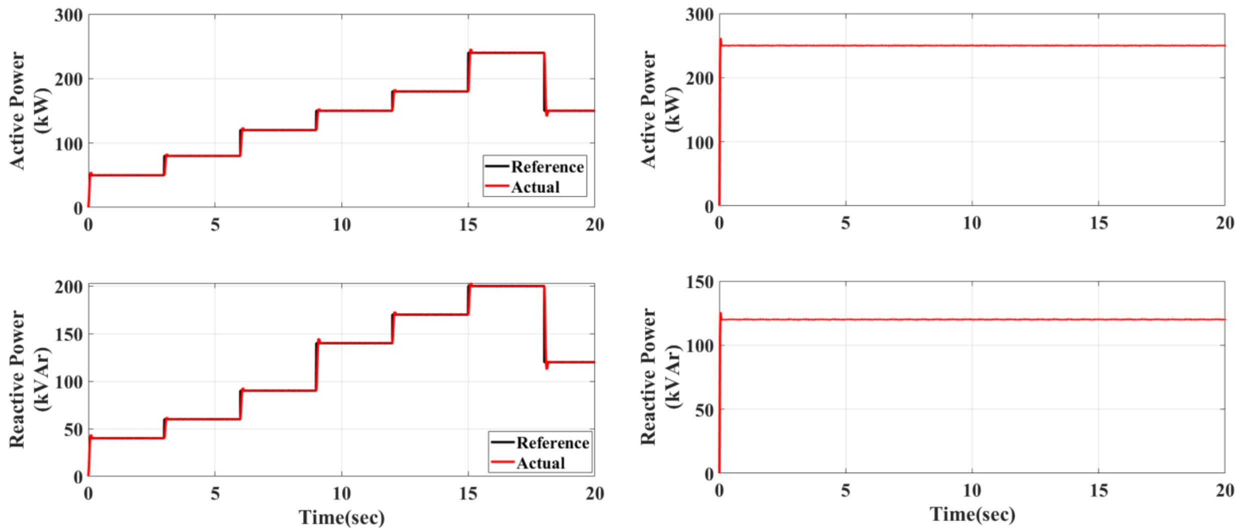

(a) *(b)*

Fig. 17. (a) Reference and actual active and reactive power converted by the VSC (b) Load active and reactive powers

The tuned PI controller ensures that the VSC closely tracks the reference power values, demonstrating the effectiveness of the GWO-optimized gains in achieving accurate power conversion. The load's active and reactive power requirements are illustrated in Fig. 17 (b). Since the converted power by the VSC exceeds the actual load demand, the surplus power is directed to the grid, as shown in Fig. 18 (a).

This highlights the system's capability to efficiently manage excess power and contribute it to the grid when required. The State of Charge (SOC) of the battery, represented in percentage, is depicted in Fig. 18 (b). During the period between 15 to 18 seconds, when the battery is in discharging mode, the SOC decreases as stored energy is used to compensate for the additional reference power demand. At all other time instances, the SOC increases as the battery remains in charging mode, storing the surplus power generated by the PV and wind systems. This controlled charging and discharging operation ensures efficient energy management and enhances the stability of the system. This case demonstrates the effectiveness of the GWO-optimized PI controller gains in regulating the power flow within the system. By maintaining constant environmental conditions, the impact of dynamically changing reference power inputs on the system's performance was evaluated. The battery efficiently transitions between charging and discharging modes based on the power demand, ensuring system stability. Furthermore, the VSC effectively tracks the reference power values, and any surplus energy is successfully transferred to the grid. The results validate the robustness of the control strategy, optimizing energy utilization while maintaining system reliability.

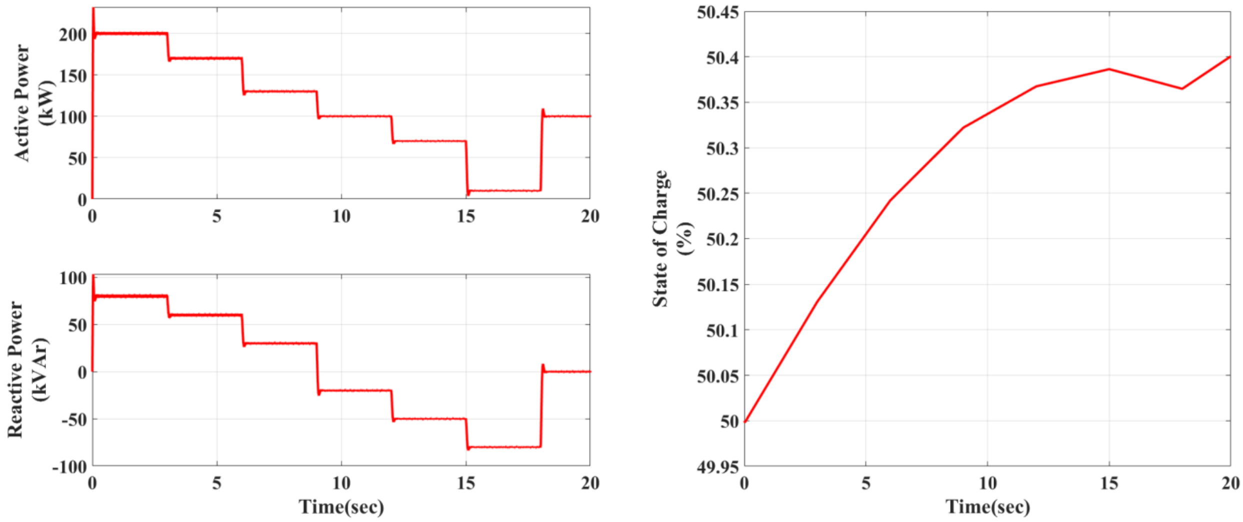

(a) *(b)*

Fig. 18. (a) Active and reactive powers provided by the grid (b) State of charge of the battery in %

6.3. Case 3: Analysis of Load Variation and System Response

In this case, the impact of load variation on system performance is analysed. The active and reactive power demands of the load fluctuate over time, as illustrated in Fig. 20 (a). The variation in load power demand is structured as follows: 0 to 3 seconds: 50 kW and 40 kVAr, 3 to 6 seconds: 120 kW and 90 kVAr, 6 to 9 seconds: 180 kW and 120 kVAr, 9 to 12 seconds: 250 kW and 240 kVAr, 12 to 15 seconds: 300 kW and 250 kVAr, 15 to 18 seconds: 220 kW and 190 kVAr, After 18 seconds: 200 kW and 180 kVAr. Unlike the previous case, where power reference values were altered, in this scenario, the irradiance, temperature, and wind speed remain constant throughout the simulation, as shown in Fig. 19 (a). Consequently, the power outputs from the PV and wind generation systems remain constant, as depicted in Fig. 19 (b).

For this case, the reference active and reactive power values are set to a constant 150 kW and 140 kVAr, respectively. Since these values remain unchanged, the power converted by the VSC also remains constant, as illustrated in Fig. 20 (a). The VSC ensures that the power delivered to the system remains at the specified reference levels, irrespective of fluctuations in the load demand. The actual active and reactive power consumption of the load is illustrated in Fig. 20 (b). Since the load demand varies over time while the VSC-converted power remains constant, a power balance mechanism is established through the interaction with the grid. The grid active and reactive power flows are depicted in Fig. 21 (a), which illustrates how the power exchange between the system and the grid occurs based on the load demand.

When the load requirement is lower than the power converted by the VSC, the surplus power is exported to the grid. Conversely, when the load requirement exceeds the power converted by the VSC, the grid supplies the additional power needed to meet the demand. This dynamic power exchange ensures that the system remains stable and that the load always receives the required power. The State of Charge (SOC) of the battery is presented in Fig. 21 (b).

Since the reference power (150 kW and 140 kVAr) is set lower than the combined power generated by the PV and wind systems, the battery remains in charging mode throughout the simulation. This results in a continuous increase in the SOC over time, as excess energy from the generation sources is stored in the battery. The charging behavior of the battery ensures efficient utilization of surplus power, preventing unnecessary wastage and enhancing system efficiency. This case demonstrates the response of the system to load variations while keeping the generation conditions constant. The VSC effectively maintains constant power conversion based on reference values, ensuring a stable power supply. The grid plays a crucial role in balancing the power demand by either absorbing surplus energy or supplying additional power when needed. The battery remains in charging mode due to the surplus energy generated from PV and wind sources, leading to an increase in SOC over time. These results highlight the system's ability to manage load fluctuations efficiently while optimizing energy utilization through battery storage and grid interaction.

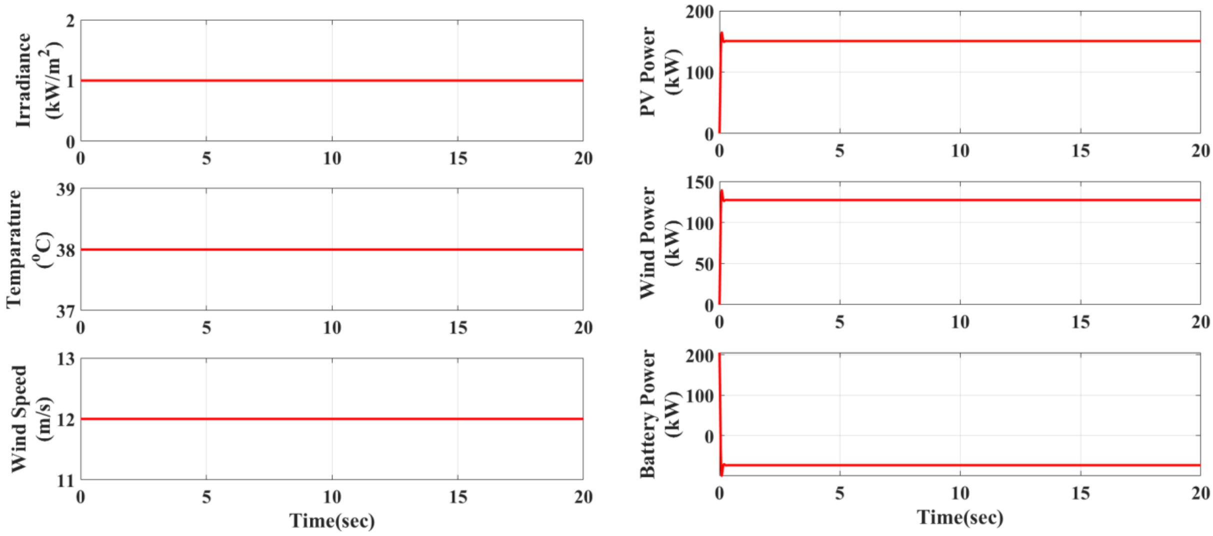

(a) *(b)*

Fig. 19. (a) Irradiance, temperature input to the PV system and wind speed input to the wind generation system (b) generated power from PV, wind and terminal power of the battery

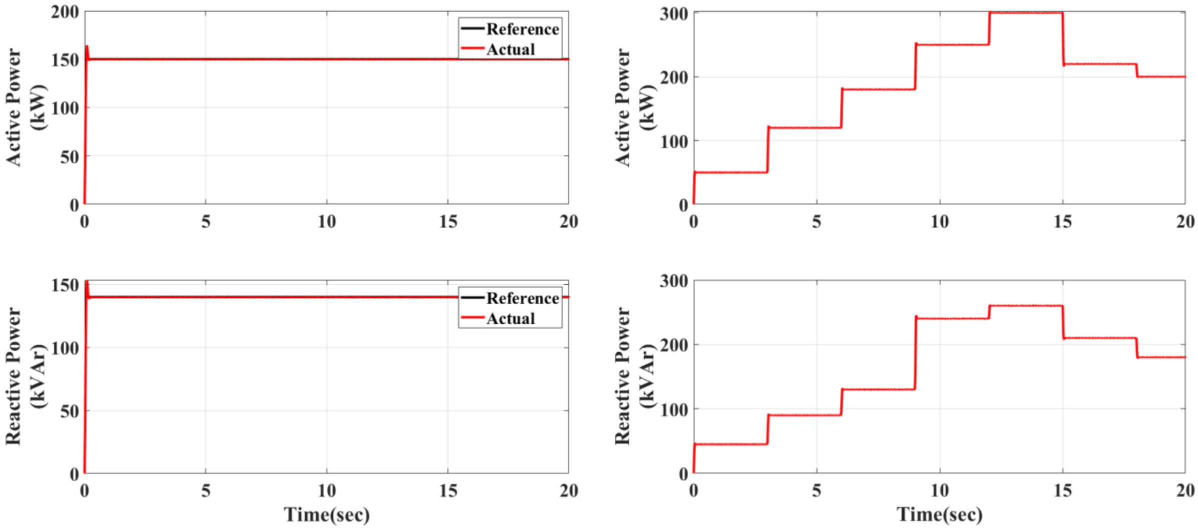

(a) *(b)*

Fig. 20. (a) Reference and actual active and reactive power converted by the VSC (b) Load active and reactive powers

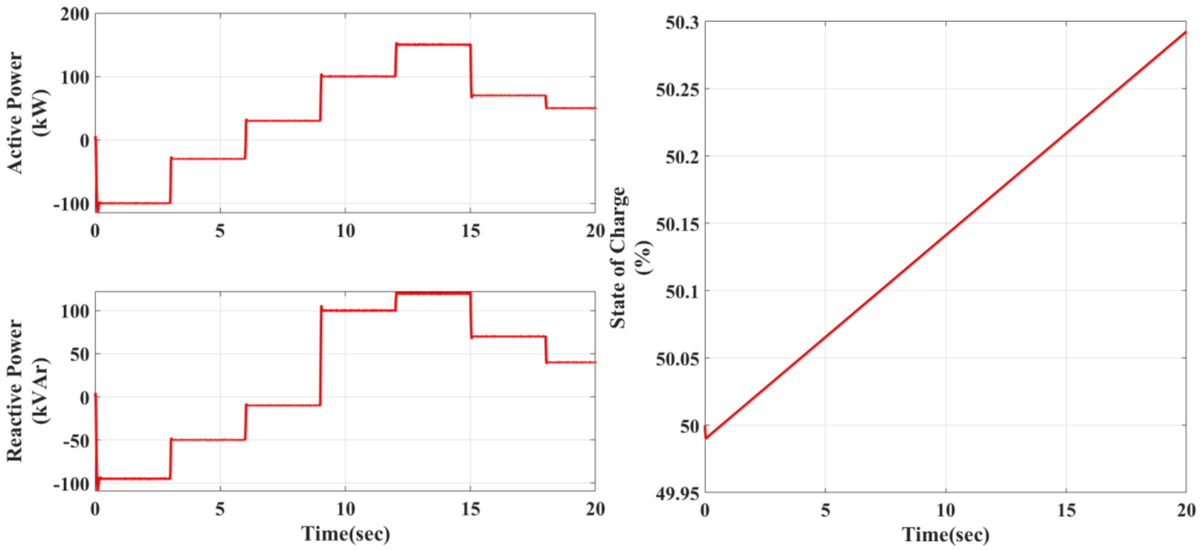

(a) *(b)*

Fig. 21. (a) Active and reactive powers provided by the grid (b) State of charge of the battery in %

7. Conclusion

This study presents the application of Grey Wolf Optimization (GWO) for tuning Proportional-Integral (PI) controllers in a PV-Wind-Battery-based microgrid to enhance power flow control and DC link voltage regulation. The integration of renewable energy sources introduces dynamic and nonlinear variations in power generation, making conventional PI tuning methods inadequate for achieving optimal system performance. To address this challenge, the GWO algorithm is employed to optimize the PI controller gains, leveraging its superior exploration and exploitation capabilities. The proposed GWO-tuned PI controllers are implemented in the Voltage Source Converter (VSC) control strategy, where active and reactive power control is adopted for efficient energy distribution. Additionally, Perturb & Observe (P&O) MPPT is used for PV power extraction, while an adaptive P&O MPPT is applied to the wind generation system to ensure maximum power tracking under varying environmental conditions. The performance of the GWO-based PI controller is evaluated through extensive simulations and is compared with conventional Ziegler-Nichols (ZN), Genetic Algorithm (GA), and Particle Swarm Optimization (PSO) based tuning approaches. Simulation results demonstrate that the GWO-optimized PI controllers significantly improve dynamic response, steady-state accuracy, and power balance within the microgrid. The optimized controllers achieve faster response times, reduced overshoot, and improved DC link voltage stability, leading to enhanced system reliability. Furthermore, battery charging and discharging behaviour is effectively regulated based on real-time power generation and load variations, ensuring efficient energy management. The GWO-based PI tuning approach proves to be an effective optimization technique for power flow control and DC link voltage regulation in microgrid systems with multiple renewable energy sources. The findings of this study contribute to the advancement of intelligent microgrid control strategies, enabling more resilient, stable, and efficient integration of renewable energy into modern power systems. Future work can explore hybrid optimization techniques and real-time hardware implementation to further validate the effectiveness of GWO-based controllers in practical applications.

REFERENCES

1. Jithendranath J., Debapriya D., Josep M.G. (2021) Probabilistic optimal power flow in islanded microgrids with load, wind and solar uncertainties including intermittent generation spatial correlation, Energy 222, 119847.
2. Irudayaraj A.X.R., Wahab N.I.A., Veerasamy V., Premkumar M., Radzi M.A.M., Sulaiman N.B., HaesAlhelou H. (2023) Decentralized frequency control of restructured energy system using hybrid intelligent algorithm and non-linear fractional order proportional integral derivative controller, IET Renewable Power Generation, 17, 8, 2009-2037.
3. Yang X., Guan J. (2024) PI parameters tuning for frequency tracking control of wireless power transfer system based on improved whale optimization algorithm, IEEE Access, 12, 13055-13069.
4. Tu B., Wang F., Huo Y., Wang X. (2023) A hybrid algorithm of grey wolf optimizer and harris hawks optimization for solving global optimization problems with improved convergence performance, Scientific Reports, 13, 1, 22909.
5. Al Sumarmad K., Sulaiman N., Abdul Wahab N.I. Hizam H. (2023) Implementation of hybrid optimized battery controller and advanced power management control strategy in a renewable energy integrated DC microgrid, Plos one, 18, 6, 0287136.
6. Al-Tameemi Z.H.A., Lie T.T., Foo G., Blaabjerg F. (2022) Optimal coordinated control of DC microgrid based on hybrid PSO–GWO algorithm, Electricity, 3, 3, 346-364.
7. Abdelhadi H., Mahmoud A.M., Saied E.M.M., Mohamed M.A.E. (2024) Innovative hierarchical control of multiple microgrids: Cheetah meets PSO, Energy Reports, 11, 4967-4981.
8. Charadi S., Chakir H.E., Redouane A., Hasnaoui A.E., Ettaoussi M. (2023) Bi-objective optimal active and reactive power flow management in grid-connected AC/DC hybrid microgrids using metaheuristic–PSO, Clean Energy, 7, 6.
9. Hartani M.A., Rezk H., Benhammou A., Hamouda M., Abdelkhalek O., Mekhilef S., Olabi A.G. (2023) Proposed frequency decoupling-based fuzzy logic control for power allocation and state-of-charge recovery of hybrid energy storage systems adopting multi-level energy management for multi-DC-microgrids, Energy, 278, 127703.
10. Güven A.F., Yörükeren N.U.R.A.N., Tag-Eldin E., Samy M.M. (2023) Multi-objective optimization of an islanded green energy system utilizing sophisticated hybrid metaheuristic approach, IEEe Access, 11, 103044-103068..
11. Gutiérrez-Escalona J., Roncero-Clemente C., Husev O., Matiushkin O., Blaabjerg F. (2024) Artificial Intelligence in the Hierarchical Control of ac, dc and Hybrid ac/dc Microgrids–A Review, IEEE Access, 12, 157227 - 157246
12. Yakout A.H., Kotb H., Hasanien H.M., Aboras K.M. (2021) Optimal fuzzy PIDF load frequency controller for hybrid microgrid system using marine predator algorithm, IEEE Access, 9, 54220-54232.
13. Guchhait P.K., Chakraborty S., Mukherjee D., Banerjee R. (2022) Intelligent reactive power control of a renewable integrated hybrid energy system model using static synchronous compensators and soft computing techniques, Journal of King Saud University-Engineering Sciences, 36, 8, 562-571
14. Zahraoui Y., Korõtko T., Rosin A., Mekhilef S., Seyedmahmoudian M., Stojcevski A., Alhamrouni I. (2024) AI applications to enhance resilience in power systems and microgrids—A review, Sustainability, 16, 12, 4959.
15. Alremali F.A.M., Yaylacı E.K., Uluer İ. (2022) Optimization of proportional-integral controllers of grid-connected wind energy conversion system using grey wolf optimizer based on artificial neural network for power quality improvement, Advances in Science and Technology. Research Journal, 16, 3.
16. Adiche S., Larbi M., Toumi D., Bouddou R., Bajaj M., Bouchikhi N., Zaitsev I. (2024) Advanced control strategy for AC microgrids: a hybrid ANN-based adaptive PI controller with droop control and virtual impedance technique, Scientific Reports, 14, 1, 31057.
17. Han X., Ding J., Cheng H. (2024) Enhanced Multiobjective Optimization Algorithm for Intelligent Grid Management of Renewable Energy Sources, International Journal of Intelligent Systems, 2024, 1, 4541163.
18. Al-Tameemi Z.H.A., Lie T.T., Foo G., Blaabjerg F. (2022) Optimal coordinated control of DC microgrid based on hybrid PSO–GWO algorithm, Electricity, 3, 3, 346-364.
19. Bouchakour A., Zarour L., Bessous N., Bechouat M., Borni A., Zaghba L., Ghoneim S. S. (2024) MPPT algorithm based on metaheuristic techniques (PSO & GA) dedicated to improve wind energy water pumping system performance, Scientific Reports, 14, 1, 17891.
20. Mian S.H., Nazir M.S., Ahmad I., Khan S.A. (2023) Optimized nonlinear controller for fuel cell, supercapacitor, battery, hybrid photoelectrochemical and photovoltaic cells-based hybrid electric vehicles, Energy, 283, 129121.